Robust topological Hall effect driven by tunable noncoplanar magnetic state in Mn-Pt-In inverse tetragonal Heusler alloys

Bimalesh Giri,[1] Arif Iqbal Mallick,[2] Charanpreet Singh,[1] P. V. Prakash Madduri,[1] Françoise Damay,[3] Aftab Alam,[2] and Ajaya K. Nayak[1,*]

[1]*School of Physical Sciences, National Institute of Science Education and Research, HBNI, Jatni-752050, India*
[2]*Department of Physics, Indian Institute of Technology Bombay, Mumbai 400076, India*
[3]*Laboratoire Léon Brillouin, CEA-CNRS, CEA Saclay, 91191 Gif-sur-Yvette, France*

(Received 17 December 2019; revised 9 July 2020; accepted 9 July 2020; published 28 July 2020)

Manipulation of magnetic ground states by effective control of competing magnetic interactions has led to the finding of many exotic magnetic states. In this direction, the tetragonal Heusler compounds consisting of multiple magnetic sublattices and crystal symmetry favoring chiral Dzyaloshinskii-Moriya interaction (DMI) provide an ideal base to realize nontrivial magnetic structures. Here we present the observation of a large robust topological Hall effect (THE) in the multisublattice $Mn_{2-x}PtIn$ Heusler magnets. The topological Hall resistivity, which originates from the nonvanishing real space Berry curvature in the presence of nonzero scalar spin chirality, systematically decreases with decreasing the magnitude of the canting angle of the magnetic moments at different sublattices. With help of first-principle calculations, magnetic and neutron diffraction measurements, we establish that the presence of a tunable noncoplanar magnetic structure arising from the competing Heisenberg exchanges and chiral DMI from the D_{2d} symmetry structure is responsible for the observed THE. The robustness of the THE with respect to the degree of noncollinearity adds up a new degree of freedom for designing THE based spintronic devices.

DOI: 10.1103/PhysRevB.102.014449

I. INTRODUCTION

In recent times, the art of easy manipulation of noncollinear magnetic structures over collinear ones has led to a drastic shift of focus on research involving next generation spintronic devices. For instance, the topologically stable noncollinear magnetic objects, e.g., skyrmions, can be engineered effectively at significantly lower current densities, thereby providing an efficient way to manipulate the information stored in these logic/spintronic devices [1–4]. In most of the cases, a basic requirement for the stabilization of these noncollinear magnetic states is the presence of chiral magnetic interaction, the Dzyaloshinskii-Moriya interaction (DMI), that develops from the broken inversion symmetry in a certain class of chiral magnets [5–9] and layered thin films [10–12]. Owing to the presence of nontrivial topological configurations, large topological Hall effect (THE) has been reported in these systems [12–17]. The basis of the THE can be associated with a nonvanishing scalar spin chirality (SSC) $\chi_{ijk} = \mathbf{S_i} \cdot (\mathbf{S_j} \times \mathbf{S_k})$ that corresponds to the solid angle Ω subtended by three spins $\mathbf{S}_i$, $\mathbf{S}_j$, and $\mathbf{S}_k$ on a unit sphere. Although measurement of THE has been extensively used to characterize topological magnetic objects, the manipulation of THE for its direct use in spintronics is never demonstrated.

For the realization of THE, the system must exhibit a nonvanishing scalar spin chirality, which can appear in magnetic materials with noncollinear and noncoplanar spin structures [18–20]. However, the lack of chiral magnetic symmetry can force a net vanishing THE in most of these systems. Rare examples of nonzero SSC has been reported in systems with special lattice structures such as pyrochlore, triangular lattices, etc., with distinctive type of spin configurations [18,21,22]. Recent observation of THE in a perpendicularly magnetized system with interfacial DMI corroborates the importance of chiral magnetic interaction to achieve a nonzero THE [23]. Along this direction, only limited experimental findings are reported in recent literature. Our particular interest is Mn based tetragonal Heusler materials well known for their potential use in the field of spintronics [9,24–26]. In this family of materials, a flexible tuning of the magnetic properties, such as magnetization, magnetic anisotropy, and Curie temperature (T_C), can be realized by tuning the sublattice magnetic moments. In addition, the noncentrosymmetric tetragonal Mn_2YZ compounds (where Y = Pt, Rh, Ir, and Ni) crystallizing in the space group $I\bar{4}m2$ are potential candidates to host DMI that can give chiral magnetic interaction in the system [9,26–28]. To realize our goal, we select the inverse tetragonal Heusler compound Mn_2PtIn as a starting compound that consists of two magnetic sublattices of Mn atoms. Here we show that a tunable topological Hall effect can be achieved depending upon the degree of noncollinearity of the magnetic moments in the system.

II. RESULTS AND DISCUSSION

Calculations for different structural and magnetic configurations of the proposed $Mn_{2-x}PtIn$ systems were carried

*ajaya@niser.ac.in

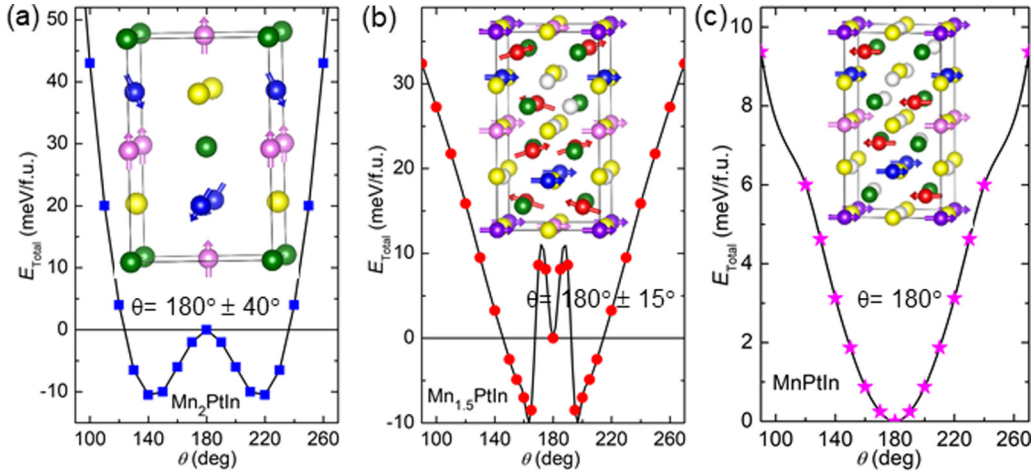

FIG. 1. First-principle calculation of magnetic structures for $Mn_{2-x}PtIn$. Total energy (with reference to $E_{\theta=180^\circ}$) versus canting angle θ of the Mn moment in (a) Mn_2PtIn, (b) $Mn_{1.5}PtIn$, and (c) MnPtIn. The alignment of magnetic moment of each Mn atom in different magnetic sublattices are shown in the inset of the respective figures. In case of Mn_2PtIn (space group $I\bar{4}m2$), Mn occupies two positions: Mn_{2b} (magenta balls) and Mn_{2d} (blue balls). For $Mn_{1.5}PtIn$ (space group $I\bar{4}2m$) and MnPtIn (space group $I\bar{4}2m$) the Mn sits at Mn_{2a} (violet balls), Mn_{2b} (magenta balls), Mn_{4d} (blue balls), and Mn_{8i} (red balls). For all cases In and Pt atoms are represented by green and yellow balls, respectively.

out to find out the energetically most favorable crystal and magnetic configurations. In case of the parent Mn_2PtIn, a minimum energy state was found for the tetragonal space group $I\bar{4}m2$. We have performed fixed-direction magnetic calculations using the noncollinear module of the Vienna *ab initio* simulation package (VASP). From the total energy as a function of canting angle of Mn moments between the alternate layers [Fig. 1(a)], it is found that Mn_2PtIn exhibits a noncollinear magnetic state characterized by canting angle of $180^\circ \pm 40^\circ$. A maximum energy scale of about 0.35 eV/formula unit (f.u.) is the energy difference between the two collinear configurations—the ferromagnetic (FM) ($\theta = 0^\circ$) and the ferrimagnetic (FiM) ($\theta = 180^\circ$). The most significant exchange coupling is between the Mn atoms in the neighboring planes, i.e., between the Mn at $2b$ and $2d$ positions. The nearest neighbor exchange coupling aligns the Mn moments of the neighboring planes ferrimagnetically. The next nearest neighbor coupling between the Mn atoms sitting in $2d$ position (Mn-Pt planes) is also significantly large and it also tries to align the Mn moments antiferromagnetically. The competition between these two interactions results in an effective canting of the Mn moments at the $2d$ position. In case of $Mn_{1.5}PtIn$ the most stable structural configuration was obtained by utilizing the experimental lattice parameters with the space group $I\bar{4}2m$. $Mn_{1.5}PtIn$ exhibits a noncollinear magnetic order characterized by canting angle of $180^\circ \pm 15^\circ$ [Fig. 1(b)] and a total uncompensated moment of about 1.13 μ_B/f.u. In case of MnPtIn, calculations were performed both for $I\bar{4}m2$ and $I\bar{4}2m$ space groups. In both cases, there can be several possible structural configurations depending on the Mn site occupancy. Irrespective of whatever magnetic configuration we start the calculation, it always stabilizes to a collinear magnetic arrangement for both space groups [Fig. 1(c)]. A net cancellation of individual moments is achieved in the case of $I\bar{4}m2$, whereas a small uncompensated magnetic moment of 0.21 μ_B/f.u. is found for $I\bar{4}2m$ space group.

Our experimental studies show that the parent Mn_2PtIn crystallizes in an inverse Heusler tetragonal phase with space group $I\bar{4}m2$ [29]. $Mn_{2-x}PtIn$ with $x = 0.2$ to 0.4 exhibit mixed structural phases due to composition dependent structural transition from the space group $I\bar{4}m2$ to $I\bar{4}2m$. Samples with $x = 0.5$ to 1.0 crystallize in the space group $I\bar{4}2m$ with a small fraction of MnPt phase for $x = 0.9$ and 1.0 [29]. The isothermal magnetization $M(H)$ loops measured at 2 K for different $Mn_{2-x}PtIn$ samples are plotted in Fig. 2(a). The saturation magnetization initially increases for $x = 0$ to 0.3 before decreasing systematically with decreasing Mn concentration. As suggested by our theoretical calculations, a fully compensated magnetic state can be found for MnPtIn that exhibit a linear kind of hysteresis loop. The variation of saturation magnetization with the Mn concentration for

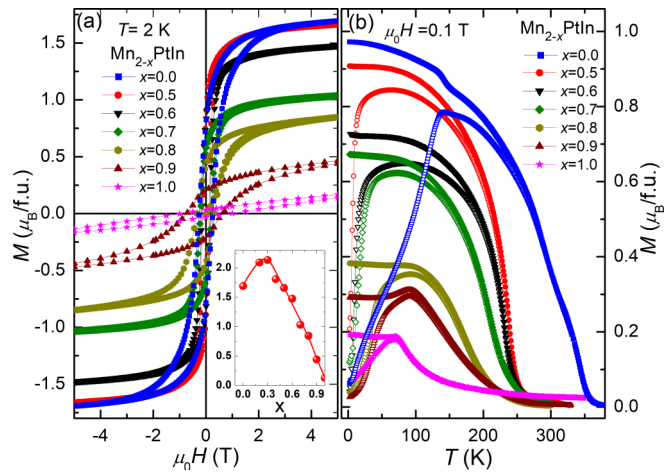

FIG. 2. (a) Field dependence of magnetization loops measured at 2 K for $Mn_{2-x}PtIn$. The inset shows compositional dependent magnetization at a field of 5 T. (b) Temperature dependence of magnetization $M(T)$ measured in zero field cooled (ZFC, open symbols) and field cooled (FC, closed symbols) modes in an applied field of 0.1 T for $Mn_{2-x}PtIn$. The $M(T)$ data for $x = 0.9$ and 1.0 are multiplied by a factor of 3 and 30, respectively, for a clear view.

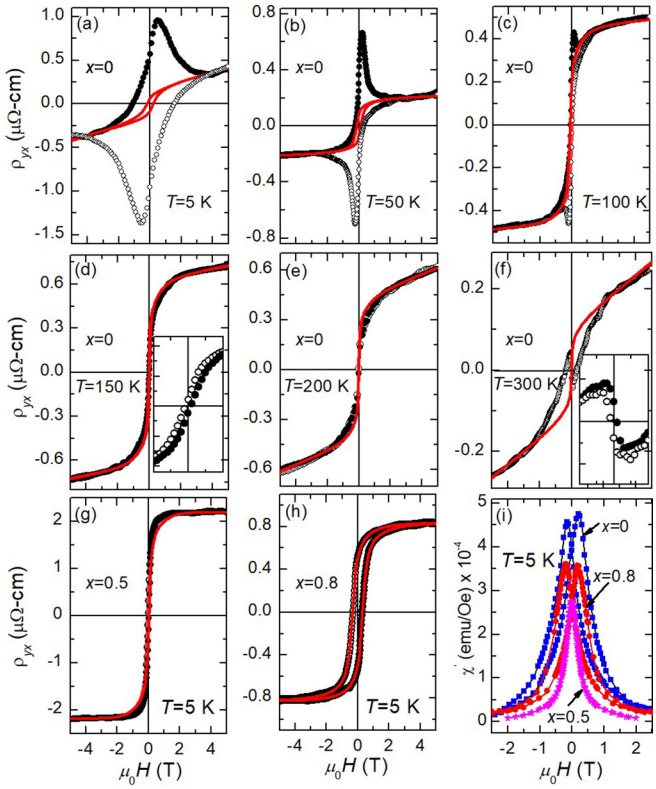

FIG. 3. Field dependence of Hall resistivity (ρ_{yx}) measured at different temperatures for (a)–(f) Mn_2PtIn, (g) $Mn_{1.5}PtIn$, and (h) $Mn_{1.2}PtIn$. The open and closed symbols represent experimental data with field sweep in $+H \rightarrow -H$ and $-H \rightarrow +H$, respectively. The solid lines corresponds to the total calculated Hall resistivity as described in the main text. (i) Field dependence of the real component of AC susceptibility, $\chi'(H)$ measured at 5 K.

$x = 0.0$ to 1.0 is plotted in the inset of Fig. 2(a). The temperature dependence of the magnetization for the $Mn_{2-x}PtIn$ are shown in Fig. 2(b). As it can be seen, the Curie temperature (T_C) systematically decreases with decreasing Mn concentration.

Our theoretical calculations and experimental studies suggest the presence of a tunable noncollinear magnetic state in the present system. To explore the effect of this noncollinearity, we have carried out a detailed Hall resistivity (ρ_{yx}) measurement for Mn_2PtIn as plotted in Figs. 3(a)–3(f). It is noteworthy to mention here that an asymmetric behavior of ρ_{yx} at $T = 5$ K mainly arises due to small longitudinal magnetoresistance contribution at this temperature, whereas no such effect is found for $T \geqslant 50$ K. The total Hall resistivity in a system can be written as $\rho_{yx} = \rho_N + \rho_{AH} + \rho_{yx}^T$, where ρ_N, ρ_{AH}, and ρ_{yx}^T are normal, anomalous, and topological Hall resistivities, respectively. The normal Hall resistivity which is linearly proportional to the magnetic field can be expressed as $\rho_N = R_0 H$, where R_0 is the normal Hall coefficient and H is the magnetic field. In a FM/FiM system, the intrinsic contribution to the anomalous Hall effect can be illustrated as $\rho_{AH} = b\rho_{xx}^2 M$, where b is a constant, ρ_{xx} is the longitudinal resistivity, and M is the magnetization. As can be seen from the experimental Hall resistivity data, at higher fields ρ_{yx} almost saturates with fields. So it can be assumed that the high field data only consists of the normal and anomalous Hall components. Therefore, ρ_{yx} at high fields can be written as $\rho_{yx} = R_0 H + b\rho_{xx}^2 M$. The calculated Hall resistivity curves for different samples and temperatures sans topological Hall resistivity are plotted as solid lines in Figs. 3(a)–3(h). In the case of Mn_2PtIn, a significant difference between the experimental and calculated Hall resistivity data can be found for temperatures up to 100 K [Figs. 3(a)–3(c)], where the ρ_{yx} data exhibit a negative hysteresis loop. This suggests that for a temperature range of 5 to 100 K, the additional scattering of the conduction electrons takes place opposite to that of normal and anomalous Hall contribution. For $T \geqslant 150$ K, the experimental ρ_{yx} data exhibit a positive hysteresis loop as shown in the inset of Figs. 3(d) and 3(f). We also observe a reasonable difference between the experimental and calculated Hall resistivity data for $Mn_{1.5}PtIn$ as shown in Fig. 3(g), whereas both curves match well for $Mn_{1.2}PtIn$, signifying the absence of any additional component of ρ_{yx} for this sample [Fig. 3(h)].

To further understand the source of the observed anomaly in the Hall data, we have performed field dependent AC-susceptibility measurements at 5 K for all the three samples [Fig. 3(i)]. The $\chi'(H)$ curves do not exhibit any kind of anomaly up to a field of ± 5 T. It can be mentioned here that all skyrmion hosting bulk materials display dip/kink kind of features in the AC-susceptibility measurements [7,26,30–32]. In addition, the first derivative of magnetization with respect to field for the $M(H)$ loops also do not exhibit any unusual behavior [29]. Therefore, it is very unlikely that the present samples possess any kind of skyrmionic phase.

The calculated ρ_{yx} ($= \rho_N + \rho_{AH}$) was subtracted from the experimental total Hall resistivity to obtain the topological Hall ρ_{yx}^T. For Mn_2PtIn, it is found that for $T \leqslant 100$ K, the maximum value of ρ_{yx}^T lies in the first and the third quadrants, whereas the maxima lies in the second and fourth quadrants for $T \geqslant 150$ K [Fig. 4(a)]. A large ρ_{yx}^T of about 1 $\mu\Omega$ cm can be found at 5 K in Mn_2PtIn. The ρ_{yx}^T drastically decreases to about 0.3 $\mu\Omega$ cm in the case of $Mn_{1.5}PtIn$ before vanishing for $Mn_{1.2}PtIn$, as depicted in the inset of Fig. 4(a). Most importantly, ρ_{yx}^T displays a strong correlation with the magnitude of canting angle in the system. To understand the change in sign of the ρ_{yx}^T above 150 K for Mn_2PtIn, we have plotted a maximum value of ρ_{yx}^T taken from the field sweep $-H \rightarrow +H$ at different temperatures [Fig. 4(b)]. The origin of the change in sign of the ρ_{yx}^T can be attributed to the existence of a spin-reorientation-like transition at 150 K as can be visualized in ZFC and FC $M(T)$ curves shown earlier in Fig. 2(b). In the case of $Mn_{1.5}PtIn$, the maximum value of ρ_{yx}^T monotonically decreases with temperature, whereas it remains almost close to zero at all temperatures for $Mn_{1.2}PtIn$. It is important to mention here that the $M(T)$ data for both $Mn_{1.5}PtIn$ and $Mn_{1.2}PtIn$ do not exhibit any kind of anomaly [see Fig. 2(b)].

Finally, to experimentally verify the existence of noncollinear magnetic structure in the present system, we have performed powder neutron diffraction (ND) experiment on $Mn_{1.5}PtIn$. The ND patterns taken in the temperature range of 1.5 to 300 K at different 2θ values are depicted in Fig. 5(a). The temperature dependent ND patterns show an increase in the scattering intensity below the ordering temperature at

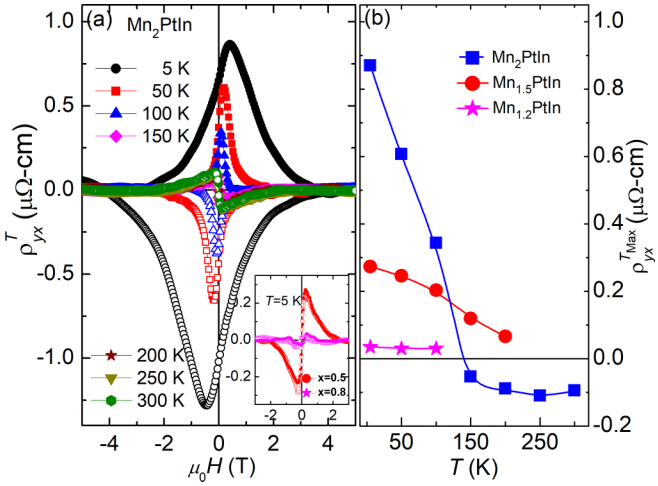

FIG. 4. (a) Topological Hall resistivity (ρ_{yx}^{T}) calculated at different temperatures for Mn_2PtIn. The open and closed symbols represent experimental data with field sweep in $+H \rightarrow -H$ and $-H \rightarrow +H$, respectively. The inset shows calculated ρ_{yx}^{T} at 5 K for $Mn_{1.5}PtIn$ (filled circles) and $Mn_{1.2}PtIn$ (filled stars) in $\mu\Omega$ cm. (b) Maximum value of ρ_{yx}^{T} as a function of temperatures (solid symbols) taken from the field dependent ρ_{yx}^{T} data.

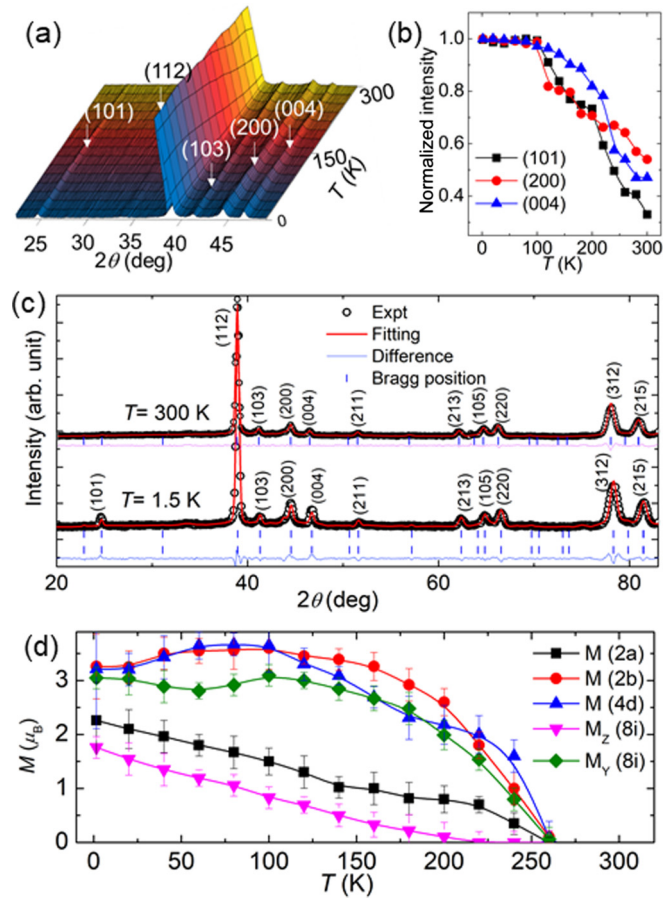

FIG. 5. (a) Neutron diffraction patterns for $Mn_{1.5}PtIn$ measured at different temperatures. For a clear view of the major magnetic reflections the patterns are shown in the 2θ range of 22 to 50 deg. (b) Temperature variation of normalized integrated intensity for the three major magnetic reflections (101), (200), and (004). (c) Rietveld refinement of the neutron diffraction patterns at 300 and 1.5 K for $Mn_{1.5}PtIn$. (d) Temperature dependence of net magnetic moment of site-specific Mn atoms at different sublattices as depicted by different symbols.

the nuclear Bragg peaks (101), (200), and (004), suggesting a commensurate magnetic structure. This can be clearly seen from the temperature variation of normalized intensities which decrease significantly with increasing temperature, suggesting the presence of contribution from both in-plane and out-of-plane magnetic components [Fig. 5(b)]. Since $Mn_{1.5}PtIn$ exhibits a T_C of about 240 K, the ND pattern at 300 K is used for the nuclear refinement by utilizing the previously determined space group $I\bar{4}2m$ (SG No. 121) and related structural parameters [Fig. 5(c), upper panel]. Furthermore, we obtained the magnetic propagation vector $k = (0, 0, 0)$ with best agreement factors by using the k-search program included in Fullprof-suite package. The Rietveld refinement of 1.5 K ND data convincingly demonstrates the presence of magnetic contribution in $Mn_{1.5}PtIn$ [Fig. 5(c), lower panel]. The temperature dependence of absolute values of the magnetic moments for Mn sitting at different sublattices are shown in Fig. 5(d). The Mn sitting at $2b$, $4d$, and $8i$ display almost equal magnitudes of magnetic moments with similar temperature dependence. The Mn moments at $2a$, $2b$, and $4d$ exhibit a complete in-plane orientation, whereas $8i$ Mn atoms possess both in-plane and out-of-plane magnetic components. A smaller magnitude of $2a$ Mn moment is due to the fact that the $2a$ site is comparatively less occupied in the present sample. More details about the analysis of ND data can be found from the Supplemental Material [29].

Our theoretical calculation and experimental results have convincingly established the presence of noncoplanar magnetic state in the present system. For a better understanding of the present THE that originates from the nonvanishing scalar spin chirality, we have considered one Mn spin ($\mathbf{S_1}$) in the Mn-In plane (plane 1) and two Mn spins ($\mathbf{S_2}$ and $\mathbf{S_3}$) from two different Mn-Pt planes (planes 2 and 3) as shown in Fig. 6(a). For simplicity, first we consider the components of the canted spins $\mathbf{S_2}$ and $\mathbf{S_3}$ lie in y-z plane. The magnetic moment of Mn atoms sitting in planes 1, 2, and 3 can be described by $\mathbf{S_1} = \mathbf{Z_1\ k}$, $\mathbf{S_2} = \mathbf{Y_2\ j} - \mathbf{Z_2\ k}$, $\mathbf{S_3} = -\mathbf{Y_2\ j} - \mathbf{Z_2\ k}$, respectively. Here Y_2 is the component of the Mn moment in the y direction and Z_1 and Z_2 are that of z direction. $\mathbf{i}, \mathbf{j}, \mathbf{k}$ are the unit vectors. For the said configuration the scalar spin chirality can be calculated as $\chi_{123} = \mathbf{S_1} \cdot (\mathbf{S_2} \times \mathbf{S_3}) = 0$. However, the competing antiferromagnetic interactions along with the chiral DMI in the system and/or the external magnetic field can tilt the in-plane component of the $\mathbf{S_2}$ and $\mathbf{S_3}$ in any direction in the ab plane. Hence, with a small x component δ, $\mathbf{S_2} = \delta\mathbf{i} + \mathbf{Y_2 j} - \mathbf{Z_2 k}$ and $\mathbf{S_3} = \delta\mathbf{i} - \mathbf{Y_2 j} - \mathbf{Z_2 k}$. As a result, we can achieve a nonvanishing $\mathbf{S_1} \cdot (\mathbf{S_2} \times \mathbf{S_3}) = -\mathbf{2Y_2 Z_1}\delta$ that can give rise to the observed topological Hall effect. As schematically depicted in Fig. 6(b), any three noncoplanar spins $\mathbf{S_i}$, $\mathbf{S_j}$, and $\mathbf{S_k}$ can subtend a solid angle Ω, thereby resulting in a nonzero scalar spin chirality with a fictitious magnetic field as shown by blue arrow. In the absence of any fixed chirality, this magnetic field will act in all possible directions, resulting in a net vanishing THE. However, the D_{2d}

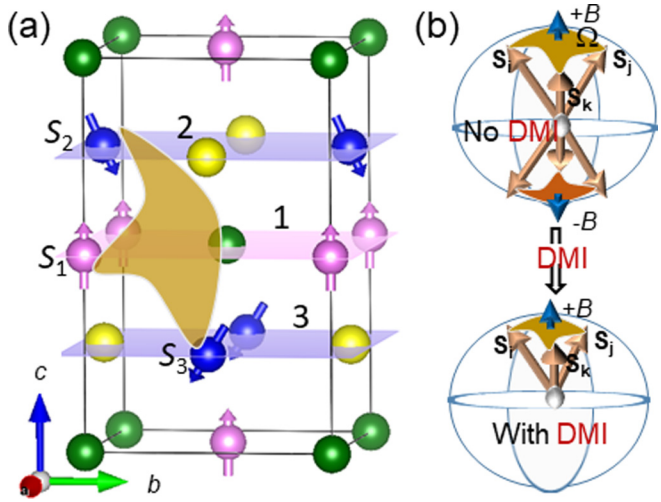

FIG. 6. (a) Unit cell for Mn_2PtIn representing Mn moments at different lattice planes. Mn-In and Mn-Pt lattice planes are shown in light magenta color marked by 1 and light blue color marked by 2 and 3, respectively. Solid angle sustained by three moments $\mathbf{S_1}$, $\mathbf{S_2}$, and $\mathbf{S_3}$ is shown in dark yellow color. (b) Upper panel: Solid angle Ω subtended by three noncoplanar spins $\mathbf{S_i}$, $\mathbf{S_j}$, $\mathbf{S_k}$ that gives a fictitious magnetic field in both upward and downward direction (blue arrows) in the absence of any chiral DMI. Lower panel: Fixed chirality in the presence of DMI.

symmetry of the present materials ensures a chiral magnetic state, thereby a nonvanishing THE in the system. At very high magnetic fields the Zeeman energy can easily overcome the chiral DMI energy, suppressing the chirality as well as the THE.

Our assertion of large topological Hall resistivity at low temperatures as a result of finite scalar spin chirality instead of any skyrmion phase is supported by several facts. (i) We do not observe any kind of kink/peak behavior in the AC-susceptibility measurements as discussed earlier. (ii) The isostructural Heusler compounds $Mn_{1.4}Pt_{0.9}Pd_{0.1}Sn$ [9] and $Mn_2Rh_{0.9}Ir_{0.1}Sn$ [33] found to exhibit antiskyrmion phase with an antiskyrmion size of about 150 and 200 nm, respectively. Since the magnitude of THE is inversely proportional to the skyrmion size (density), it is expected that the antiskyrmion phase in these systems will result in topological Hall resistivity in the order of 1 nΩ cm or less. (iii) It can be clearly seen that Mn_2PtIn displays a spin-reorientation transition around 150 K. The previous studies on similar systems show the existence of antiskyrmion phase, if any, only above the spin-reorientation transition [9,32].

The noncoplanar spin structure with finite scalar spin chirality as a source of THE has been recently observed in FM systems [23], as well as in antiferromagnetic systems (AFM) [34]. Although THE arises in systems hosting skyrmions/antiskyrmions or comprised of noncoplanar spin structures, a very basic difference lies in the length scale of the periodicity associated with their magnetic structure. A crossover between a long periodic magnetic structure to a comparatively shorter scale noncoplanar magnetic state is about interplay between the energy contributions from various energy terms [35]. In the case of the present systems under study, it might be possible to stabilize a incommensurately modulated helical/cycloid ground state with a modulation period up to a few hundred. These helix/cycloid can transform into skyrmions/antiskyrmions under the external magnetic field and in turn can cause very small THE due to the large size of the skyrmions. In a recent study, Kumar *et al.* have assigned the low temperature THE in some of their samples to the presence of antiskyrmions, although these samples display a large canting angle below the spin-reorientation transition [36]. However, the THE is only found when there is a large canting angle, indicating its probable origin from the nonvanishing scalar spin chirality coming from the noncoplanar magnetic state. This scenario is supported by the nonexistence of any THE in the well-established antiskyrmion phase, probably due to the large size of the antiskyrmions in these materials.

III. CONCLUSION

In summary, our theoretical calculations as well as experimental findings convincingly establish the presence of noncollinear magnetic ground states, resulting in a robust THE. We show a controlled tuning of the topological Hall effect by modifying the canted magnetic state in the system. The magnitude of the spin canting achieved by tuning the Mn composition is associated with a small change in lattice parameters that eventually controls various fundamental parameters such as the exchange interactions, the DMI, and the magnetocrystalline anisotropy (MCA). Hence, the competition among these parameters determines the underlying magnetic texture of the present system. Therefore, the THE in the present case can be controlled electrically by inducing strain in the system. Hence, the present study on realization of tunable THE possesses a great potential in all electrical switching based memory application. A very recent study on electrical control of an anomalous Hall state corroborates the importance of the present study that can motivate further research in this direction [37].

ACKNOWLEDGMENTS

A.K.N. acknowledges the support from Department of Atomic Energy (DAE), the Department of Science and Technology (DST)-Ramanujan research grant (Grant No. SB/S2/RJN-081/2016), SERB research grant (Grant No. ECR/2017/000854), and Nanomission research grant [Grant No. SR/NM/NS-1036/2017(G)] of the Government of India. A.A. thanks IRCC, IIT Bombay for supporting this research through Early Carrier Award Grant, Code: RI/0217/10001338-001.

[1] F. Jonietz, S. Mühlbauer, C. Pfleiderer, A. Neubauer, W. Münzer, A. Bauer, T. Adams, R. Georgii, P. Böni, R. A. Duine, K. Everschor, M. Garst, and A. Rosch, Science **330**, 1648 (2010).

[2] X. Z. Yu, N. Kanazawa, W. Z. Zhang, T. Nagai, T. Hara, K. Kimoto, Y. Matsui, Y. Onose, and Y. Tokura, Nat. Commun. **3**, 988 (2012).

[3] N. Nagaosa and Y. Tokura, Nat. Nanotechnol. **8**, 899 (2013).

[4] A. Fert, V. Cros, and J. Sampaio, Nat. Nanotechnol. **8**, 152 (2013).

[5] S. Mühlbauer, B. Binz, F. Jonietz, C. Pfleiderer, A. Rosch, A. Neubauer, R. Georgii, and P. Böni, Science **323**, 915 (2009).

[6] X. Z. Yu, Y. Onose, N. Kanazawa, J. H. Park, J. H. Han, Y. Matsui, N. Nagaosa, and Y. Tokura, Nature (London) **465**, 901 (2010).

[7] S. Seki, X. Z. Yu, S. Ishiwata, and Y. Tokura, Science **336**, 198 (2012).

[8] C. Jin, Z.-A. Li, A. Kovacs, J. Caron, F. Zheng, F. N. Rybakov, N. S. Kiselev, H. Du, S. Blügel, M. Tian, Y. Zhang, M. Farle, and R. E. Dunin-Borkowski, Nat. Commun. **8**, 15569 (2017).

[9] A. K. Nayak, V. Kumar, T. Ma, P. Werner, E. Pippel, R. Sahoo, F. Damay, U. K. Rößler, C. Felser, and S. S. P. Parkin, Nature (London) **548**, 561 (2017).

[10] S. Heinze, K. von Bergmann, M. Menzel, J. Brede, A. Kubetzka, R. Wiesendanger, G. Bihlmayer, and S. Bügel, Nat. Phys. **7**, 713 (2011).

[11] A. Soumyanarayanan, M. Raju, A. L. G. Oyarce, A. K. C. Tan, M.-Y. Im, A. P. Petrović, P. Ho, K. H. Khoo, M. Tran, C. K. Gan, F. Ernult, and C. Panagopoulos, Nat. Mater. **16**, 898 (2017).

[12] M. Raju, A. Yagil, A. Soumyanarayanan, A. K. C. Tan, A. Almoalem, F. Ma, O. M. Auslaender, and C. Panagopoulos, Nat. Commun. **10**, 696 (2019).

[13] S. R. Saha, H. Sugawara, T. D. Matsuda, H. Sato, R. Mallik, and E. V. Sampathkumaran, Phys. Rev. B **60**, 12162 (1999).

[14] A. Neubauer, C. Pfleiderer, B. Binz, A. Rosch, R. Ritz, P. G. Niklowitz, and P. Böni, Phys. Rev. Lett. **102**, 186602 (2009).

[15] N. Kanazawa, Y. Onose, T. Arima, D. Okuyama, K. Ohoyama, S. Wakimoto, K. Kakurai, S. Ishiwata, and Y. Tokura, Phys. Rev. Lett. **106**, 156603 (2011).

[16] J. C. Gallagher, K. Y. Meng, J. T. Brangham, H. L. Wang, B. D. Esser, D. W. McComb, and F. Y. Yang, Phys. Rev. Lett. **118**, 027201 (2017).

[17] T. Kurumaji, T. Nakajima, M. Hirschberger, A. Kikkawa, Y. Yamasaki, H. Sagayama, H. Nakao, Y. Taguchi, T. Arima, and Y. Tokura, Science **365**, 914 (2019).

[18] Y. Taguchi, Y. Oohara, H. Yoshizawa, N. Nagaosa, and Y. Tokura, Science **291**, 2573 (2001).

[19] H. Ishizuka and N. Nagaosa, Sci. Adv. **4**, eaap9962 (2018).

[20] P. K. Rout, P. V. P. Madduri, S. K. Manna, and A. K. Nayak, Phys. Rev. B **99**, 094430 (2019).

[21] Y. Machida, S. Nakatsuji, Y. Maeno, T. Tayama, T. Sakakibara, and S. Onoda, Phys. Rev. Lett. **98**, 057203 (2007).

[22] H. Takatsu, S. Yonezawa, S. Fujimoto, and Y. Maeno, Phys. Rev. Lett. **105**, 137201 (2010).

[23] W. Wang, M. W. Daniels, Z. Liao, Y. Zhao, J. Wang, G. Koster, G. Rijnders, C.-Z. Chang, D. Xiao, and W. Wu, Nat. Mater. **18**, 1054 (2019).

[24] T. Graf, C. Felser, and S. S. Parkin, Prog. Solid State Chem. **39**, 1 (2011).

[25] A. K. Nayak, M. Nicklas, S. Chadov, P. Khuntia, C. Shekhar, A. Kalache, M. Baenitz, Y. Skourski, V. K. Guduru, A. Puri, U. Zeitler, J. M. D. Coey, and C. Felser, Nat. Mater. **14**, 679 (2015).

[26] S. Sen, C. Singh, P. K. Mukharjee, R. Nath, and A. K. Nayak, Phys. Rev. B **99**, 134404 (2019).

[27] A. K. Nayak, C. Shekhar, J. Winterlik, A. Gupta, andC. Felser, Appl. Phys. Lett. **100**, 152404 (2012).

[28] O. Meshcheriakova, S. Chadov, A. K. Nayak, U. K. Rößler, J. Kübler, G. André, A. A. Tsirlin, J. Kiss, S. Hausdorf, A. Kalache, W. Schnelle, M. Nicklas, and C. Felser, Phys. Rev. Lett. **113**, 087203 (2014).

[29] See Supplemental Material at http://link.aps.org/supplemental/10.1103/PhysRevB.102.014449 for details of sample preparation, characterization, magnetic and transport measurements, and neutron diffraction analysis, which includes Refs. [15,38–46].

[30] H. Wilhelm, M. Baenitz, M. Schmidt, U. K. Rössler, A. A. Leonov, and A. N. Bogdanov, Phys. Rev. Lett. **107**, 127203 (2011).

[31] A. Bauer and C. Pfleiderer, Phys. Rev. B **85**, 214418 (2012).

[32] Sk Jamaluddin, S. K. Manna, B. Giri, P. V. Prakash Madduri, S. S. P. Parkin, and A. K. Nayak, Adv. Funct. Mater. **29**, 1901776 (2019).

[33] J. Jena, R. Stinshoff, R. Saha, A. K. Srivastava, T. Ma, H. Deniz, P. Werner, C. Felser, and S. S. P. Parkin, Nano Lett. **20**, 59 (2020).

[34] C. Sürgers, G. Fischer, P. Winkel, and H. von Löhneysen, Nat. Commun. **5**, 3400 (2014).

[35] A. N. Bogdanov, U. K. Rößler, M. Wolf, and K.-H. Müller, Phys. Rev. B **66**, 214410 (2002).

[36] V. Kumar, N. Kumar, M. Reehuis, J. Gayles, A. S. Sukhanov, A. Hoser, F. Damay, C. Shekhar, P. Adler, and C. Felser, Phys. Rev. B **101**, 014424 (2020).

[37] H. Tsai, T. Higo, K. Kondou, T. Nomoto, A. Sakai, A. Kobayashi, T. Nakano, K. Yakushiji, R. Arita, S. Miwa, Y. Otani, and S. Nakatsuji, Nature (London) **580**, 608 (2020).

[38] G. Kresse and J. Furthmuller, Phys. Rev. B **54**, 11169 (1996); Comput. Mater. Sci. **6**, 15 (1996).

[39] G. Kresse and D. Joubert, Phys. Rev. B **59**, 1758 (1999).

[40] L. Pál, E. Krén, G. Kádár, P. Szabó, and T. Tarnóczi, J. Appl. Phys. **39**, 538 (1968).

[41] A. S. Wills, Physica B **276**, 680 (2000).

[42] N. Nagaosa, J. Sinova, S. Onoda, A. H. MacDonald, and N. P. Ong, Rev. Mod. Phys. **82**, 1539 (2010).

[43] Y. Tian, L. Ye, and X. Jin, Phys. Rev. Lett. **103**, 087206 (2009).

[44] S. X. Huang and C. L. Chien, Phys. Rev. Lett. **108**, 267201 (2012).

[45] K. Ueda, R. Kaneko, H. Ishizuka, J. Fujioka, N. Nagaosa, and Y. Tokura, Nat. Commun. **9**, 3032 (2018).

[46] M. Lee, Y. Onose, Y. Tokura, and N. P. Ong, Phys. Rev. B **75**, 172403 (2007).